Bioactive Materials 6 (2021) 4758–4771

Contents lists available at ScienceDirect

Bioactive Materials

journal homepage: www.sciencedirect.com/journal/bioactive-materials

Water-soluble PANI:PSS designed for spontaneous non-disruptive membrane penetration and direct intracellular photothermal damage on bacteria

Huanfeng Tang [a], Yifan Liu [a], Bing Li [a,c], Bo Shang [a], Jiacheng Yang [a], Congrou Zhang [b], Lijun Yang [b], Kezheng Chen [a,**], Wei Wang [a,***], Jianfeng Liu [a,b,*]

[a] Lab of Functional and Biomedical Nanomaterials, College of Materials Science and Engineering, Qingdao University of Science and Technology, Qingdao, 266042, China

[b] Tianjin Key Laboratory of Radiopharmacokinetics for Innovative Drugs, Chinese Academy of Medical Sciences, And Institute of Radiation Medicine, Chinese Academy of Medical Sciences & Peking Union Medical College, Tianjin, 300192, PR China

[c] State Key Laboratory of Solid Lubrication, Lanzhou Institute of Chemical Physics, Chinese Academy of Sciences, Lanzhou, 730000, PR China

ARTICLE INFO

Keywords:
Conducting polymers
Membrane penetration
Photothermal
Antibacterial

ABSTRACT

The major challenge in the field of antibacterial agents is to overcome the low-permeability of bacteria cell membranes that protects the cells against diverse drugs. In this work, water-soluble polyaniline (PANI)-poly (p-styrenesulfonic acid) (PSS) (PANI:PSS) is found to spontaneously penetrate bacteria cellular membranes in a non-disruptive way, leaving no evidence of membrane poration/disturbance or cell death, thus avoiding side effects caused by cationic ammonia groups in traditional ammonia-containing antibacterial agents. For aqueous synthesis, which is important for biocompatibility, the polymer is synthesized via an enzyme-mimetic route relying on the catalysis of a nanozyme. Owing to its fluorescent properties, the localization of as-prepared PANI:PSS is determined by the confocal microscope, and the results confirm its rapid entry into bacteria. Under 808 nm near-infrared (NIR) irradiation, the internalized PANI:PSS generates local hyperthermia and destroys bacteria highly efficiently from inside the cells due to its excellent photothermal effects. *Staphylococcus aureus* (*S. aureus*), *Methicillin-resistant Staphylococcus aureus* (*MRSA*) and *Escherichia coli* (*E. coli*) could be effectively eliminated as well as the corresponding bacterial biofilms. Results of *in vivo* antibacterial experiments demonstrate excellent antibacterial activities of the water-soluble PANI:PSS without side effects. Therefore, the prepared water-soluble polymer in this study has great potential in the treatment of various bacterial infections.

1. Introduction

With the abuse of antibiotics, the multi-drug resistance (MDR) caused by bacteria has greatly weakened the curative effect of traditional antibiotics [1–3]. According to statistics, most of the bacterial infections are caused by bacterial biofilms (BFs). BFs is formed by aggregated bacteria that secrete polysaccharide matrix, related proteins, etc., which wrap themselves up [4,5]. Studies have found that infections related to the formation of biofilms usually show strong resistance and insensitivity to antibiotics [6]. To solve these serious problems, some chemical antibacterial agents, such as heavy metal ions/oxidants [7,8], antibacterial peptides [9,10] and quaternary ammonium compounds [11–13], were used in bacterial treatment. However, these antibacterial agents still have disadvantages of varying degrees, such as high cost, poor biocompatibility, and insufficient resistance to drug resistance [14]. Therefore, the development of new antibacterial strategies for the treatment of bacterial infection-related diseases is very urgent.

Being the out barrier of bacteria, cell walls and membranes protect bacteria from various antibacterial agents. It has been demonstrated that the increase in antibacterial agents uptake greatly enhances the

Peer review under responsibility of KeAi Communications Co., Ltd.

* Corresponding author.Lab of Functional and Biomedical Nanomaterials, College of Materials Science and Engineering, Qingdao University of Science and Technology, Qingdao, 266042, China.

** Corresponding author.

*** Corresponding author.

E-mail addresses: kchen@qust.edu.cn (K. Chen), wangwei@qust.edu.cn (W. Wang), liujianfeng@irm-cams.ac.cn (J. Liu).

https://doi.org/10.1016/j.bioactmat.2021.05.019

Received 19 February 2021; Received in revised form 12 May 2021; Accepted 12 May 2021

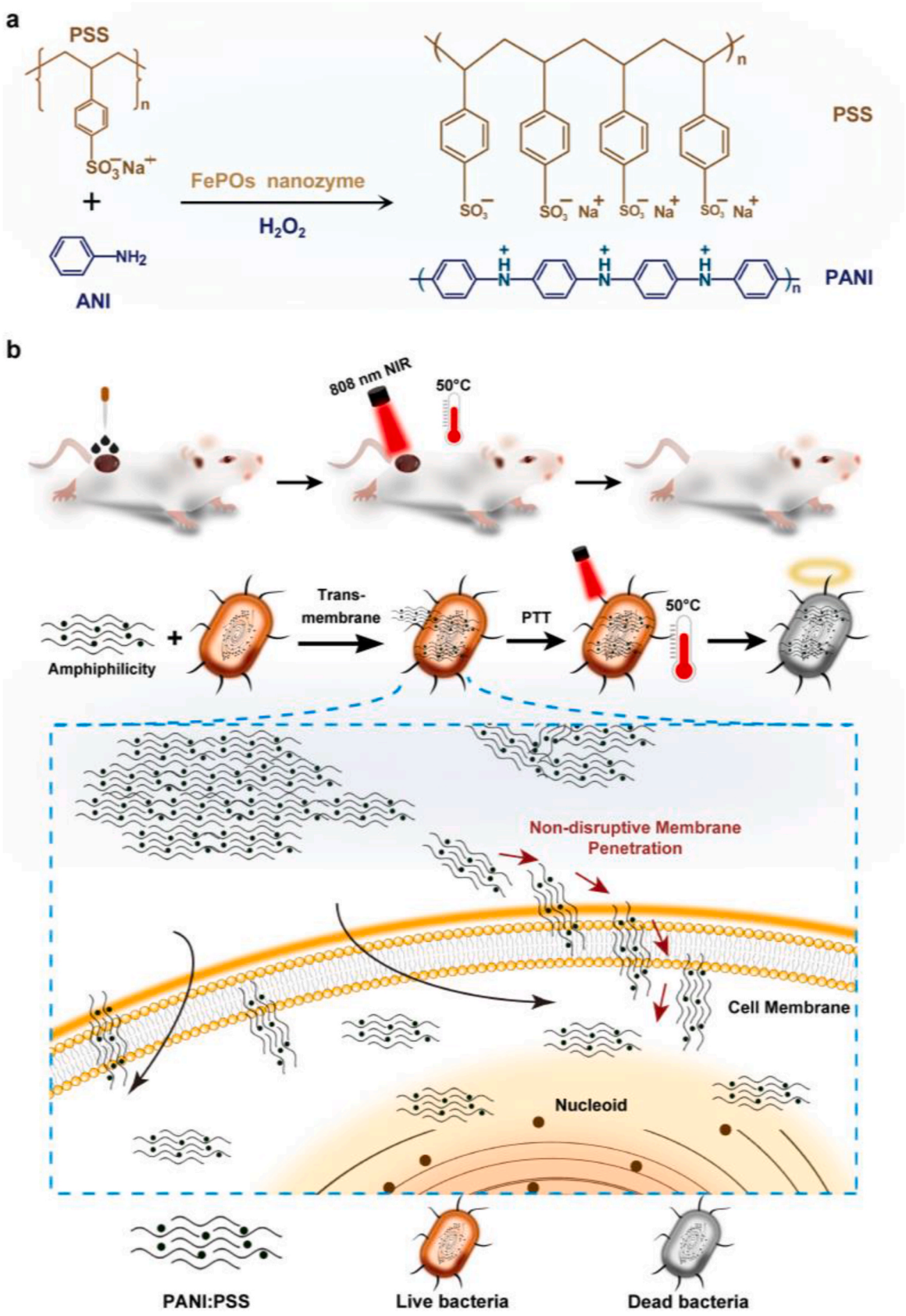

Scheme 1. Schematic illustration of (a) the synthesis protocol of water-soluble PANI:PSS and (b) the spontaneous, non-disruptive translocation and photothermal antibacterial mechanism of water-soluble PANI:PSS against *MRSA*, *S. aureus*, and *E. coli*.

antibacterial efficiency. Rapid membrane-penetrating offers straight access to bacteria chromatin and cytosol, which is followed by interrupted regulatory functions of membranes, and inactivation of proteins and DNA/RNA molecules [12,15,16]. Till now, researchers have developed several antibacterial agents that can translocate across the bacteria cell membranes using a cationic strategy based on the electrostatic attraction between the positively charged agents and negatively charged membranes [17–19]. However, the cytotoxicity of cationic compounds limits their applications since they may cause membrane disturbance of mammalian cells [20]. In contrast, a spontaneous, non-disruptive translocation may solve the problem. Inspired by the transmembrane proteins characterized by amphiphilic nature, Stellacci's group first reported the amphiphilic strategy to realize the spontaneous fusion of amphiphilic monolayer-protected gold nanoparticles (AuNPs) with lipid bilayers [21]. It is regretful that the fusion of amphiphilic AuNPs is only favorable for AuNPs with core diameters less than 10 nm as a result of the effect of particle diameter and surface composition on the fusion. Moreover, long-term toxicity relative to the slow clearance of the gold core is a big concern for clinical applications [20–22]. Herein, we report a clearable polymer antibacterial agent with the chemical composition of polyaniline (PANI)-poly (p-styrenesulfonic acid) (PSS) (PANI:PSS), which can translocate across bacteria cell membranes non-disruptively owing to its amphiphilic feature and then exert hyperthermia damage to the intracellular contents due to its excellent photothermal properties.

Photothermal antibacterial (PTA) is considered to be one of the most potential antibacterial strategies. Numerous literatures have proven that the heat converted from light energy can inhibit the growth of multidrug-resistant bacteria and also prevent the formation of bacterial biofilm structures [23]. What's more, PTA protocols are generally featured by minimal invasiveness, high tissue permeability, and negligible thermal damage under the biological window (700–1000 nm) [24,25].

PANI is a well-known conducting polymer, which has been widely studied as biosensors [26], artificial muscles [27] and neural electrodes [28] with excellent performance. In recent years, the bio-applications of PANI are further extended to the field of photothermal therapy since protonated PANI can convert NIR energy into a large amount of heat [29,30]. In addition, PANI has been successfully used as an electroactive material to study cell proliferation and proven to be non-toxic [31]. Compared to the inorganic photothermal agents, PANI has better clinical application prospects due to its good biocompatibility and degradability [32]. In spite of a number of reports on PANI with regard to its antibacterial applications [33–36], the photothermal inhibition effects were still rely on disruption of the bacterial cell walls and membranes since PANI is not normally allowed to enter and the heat is generated from outside the cells [37].

From the perspective of developing rapid efficient antibacterial protocols with minimal side effects, we report here the antibacterial performances of water-soluble PANI:PSS which is intrinsically amphiphilic thus able to realize translocation across membranes without overt membrane disruption/poration. The killing efficiency is significantly high since hyperthermia is applied directly to the most important biomolecules, i. e., chromatin and proteins, of bacteria. An enzyme-mimetic aqueous synthesis method, which is important for biological system compatibility, is chosen for the synthesis of PANI:PSS using iron phosphates (FePOs) nanozyme as the catalyst and H_2O_2 as the initiator [38]. Sulfonated polystyrene (PSS), which is the most favorable to promote the desired head-to-tail coupling of aniline monomers and water solubility of PANI:PSS, was selected as a macromolecular template to guide the biomimetic synthesis of PANI:PSS (Scheme 1).

2. Material and methods

2.1. Materials

The reagents used in the experiment: $FeCl_2{\cdot}4H_2O$ from Tianjin Bodi Chemical Co., Ltd.; polyvinylpyrrolidone (PVP), polystyrene sulfonate (PSS), and aniline monomer (98%) were from Beijing J&K Scientific Ltd.; $NaH_2PO_2{\cdot}H_2O$ came from Sinopharm Chemical Reagent Co., Ltd.; citric acid and ethylene glycol came from Tianjin No.3 Chemical Reagent Factory. 30% H_2O_2 solution was purchased from Junteng Chemical Co., Ltd (Shandong, China). Dimethyl sulfoxide (DMSO) and Triton X-100 were purchased from J&K Chemical Technology (Beijing, China). Calcein acetyl methyl ester/propidium iodide (Calcein-AM/PI) double stain kit was purchased from Yeasen Biotechnology (Shanghai, China). Hematoxylin-Eosin/H&E staining kit, Masson's Trichrome staining kit, 4′,6-diamidino-2-phenylindole (DAPI), chloral hydrate, and agar were purchased from Solarbio Technology Co., Ltd (Beijing, China). Anti-IL-6 antibody ab6672 was purchased from Abcam Company. Yeast extract and tryptone were acquired by British OXOID company. Paraformaldehyde, sodium chloride (NaCl), potassium chloride (KCl), disodium hydrogen phosphate ($Na_2HPO_4{\cdot}12H_2O$), potassium dihydrogen phosphate (KH_2PO_4), ethanol and methanol came from Tianjin Chemical Reagent Supply and Marketing. Phosphate buffer saline (PBS, pH = 7.4) was prepared by dissolving NaCl, KCl, Na_2HPO_4 and KH_2PO_4 in water. Uranium acetate and copper mesh were used by Beijing Zhongjing Science and Technology Co., Ltd. Bovine Serum Albumin (BSA) was approved by Shanghai Yisheng Biotechnology Co., Ltd. Optimal Cutting Temperature Compound (OCT) was acquired by Thermo. All commercially available chemical solvents and reagents were used without further purification. Ultrapure Milli-Q water was used to prepare the aqueous solution.

For cell culture experiments, the following reagents were used: all cells were maintained in Tianjin Key Laboratory of Radiation Medicine and Molecular Nuclear Medicine; Dulbeco's Modified Eagle's Medium (DMEM) from Gibco supplemented with 10% fetal bovine serum (FBS, Biological Industries Corporation) and 1% penicillin/streptomycin (pen/strep, Gibco) at 37 °C in 5% CO_2; trypsin-ethylene diamine tetraacetic acid (EDTA) solution and cell counting Kit-8 (CCK8) were purchased from Solarbio (Beijing, China); cell culture dishes and 96-well plates were approved by Corning.

The live animals used in the experiment were purchased from Vital River Laboratory Animal Technology Co., Ltd., and the experiments were carried out in a specific pathogen-free (SPF) environment [36].

2.2. Synthesis of FePOs nanozyme

The method reported by our group [35] was used to prepare FePOs. $FeCl_2{\cdot}4H_2O$ (198.8 mg) and $NaH_2PO_2{\cdot}H_2O$ (106.0 mg) were dissolved in dd H_2O (5 mL), and then glycol (35 mL) and PVP (1.0 g) were added under vigorous stirring. After stirring uniformly, the mixture was transferred to a polytetrafluoroethylene lined autoclave with a total volume of 50 mL, sealed at a constant temperature of 180 °C for 24 h, and then the system was naturally cooled to room temperature. The resulting product was collected, washed with dd H_2O and ethanol 5 times each, and dried under vacuum for 6 h.

2.3. Synthesis of water-soluble PANI:PSS

An enzyme-like synthesis method reported by our group [35] was used to prepare water-soluble PANI:PSS. PSS (124.0 mg) was added into citric acid (19.2 mL, 0.1 M)-Na_2HPO_4 (0.8 mL, 0.2 M) buffer (pH = 2.2), and the mixture was stirred for 30 min. Then aniline monomer (85.0 mg) was weighed and added to stir for 1 h. FePOs nanozyme (5.0 mg) and H_2O_2 (598 μL, 1.0 M) were added dropwise, heated and stirred in a constant temperature water bath (70 °C, 24 h). The product was dialyzed for 48 h by a dialysis membrane (cutoff KDa = 8000–14000) and

then lyophilized in a lyophilizer to obtain water-soluble PANI:PSS.

2.4. Characterization of water-soluble PANI:PSS

Characterization of UV–Vis–NIR absorption: The absorption spectra of the samples were recorded on a UV–Vis–NIR spectrophotometer (UV-TU-1810; Beijing Puxi General Instrument Co., Ltd.; China).

Characterization of Zeta potential and particle size: PANI:PSS was diluted in water and bacterial culture medium both to a concentration of 0.01 mg/mL, and then the Zeta potential and average hydrodynamic diameter (Dh) were characterized by a dynamic light scattering (DLS) analyzer (Zetasizer Nano ZS; Malvern Panalytical; England).

Characterization of photothermal effect: PANI:PSS aqueous solution (500 μL, 0–2.0 mg/mL) was added to 1.5 mL EP tube, and NIR irradiation (808 nm, 1.5 W/cm^2, 5 min) was performed. Every 20 s, the temperature of the PANI:PSS solution was recorded with a NIR thermal imaging camera (Fluke, Ti200; USA). In addition, the photothermal effect of water-soluble PANI:PSS with gradient concentrations in the range of 0–2.0 mg/mL was evaluated under 808 nm laser irradiation (0.33, 0.75, 1.0, 1.5 W/cm^2) for 5 min. A radiation meter (LM8, Coherent, USA) was used to measure the light intensity of the 808 nm laser (CL808-5W, Qingdao Photons Co. Ltd., China). The temperature was recorded using an online-type thermocouple thermometer (UT325, Uni-Trend Technology Co. Ltd., China).

Characterization of fluorescent properties: Fluorescent property measurement was performed at room temperature on PANI:PSS aqueous solution, using a fluorescence spectrophotometer (F4600, Hitachi; Japan), by an 808 nm diode laser as the excitation source, and with a fiber optic accessory [39].

Measurement of the photothermal conversion efficiency and cycle stability: At first, PBS (0.4 mL) was irradiated by a NIR laser (808 nm, 1.0 W/cm^2, 5 min), and then cool to room temperature under normal conditions. During this period, the temperature of the EP tube was recorded every 20 s. Then the PANI:PSS solution (0.4 mL, 1.0 mg/mL) was irradiated by the 808 nm laser (1.0 W/cm^2, 5 min), which was repeated five times. Finally, a time-temperature curve was plotted and the photothermal conversion efficiency of the PANI:PSS was calculated by the following equations [40].

$$\theta = \frac{T - T_{surr}}{T_{\max} - T_{surr}} \tag{1}$$

$$\tau_s = \frac{t}{-1n\theta} \tag{2}$$

$$hS = \frac{Cm}{\tau_s} \tag{3}$$

$$Q_{dis} = hS(T_{\max} - T_{surr}) \tag{4}$$

$$n = \frac{hS(T_{\max} - T_{surr}) - Q_{dis}}{I\left(1 - 10^{-A808}\right)} \tag{5}$$

where η is the PANI:PSS photothermal conversion efficiency value, $T_{\max}$ is the highest temperature of the measurement solution, T_{surr} is the ambient temperature, A_{808} is the absorbance of the PANI:PSS solution at 808 nm, Q_{dis} is the heat emitted to the environment, C is the specific heat capacity of water, m is the mass of the solution, and T is the real-time temperature of the measured solution, t is the time, τ_s is the slope of the fitting straight line of the temperature drop curve of the PANI:PSS solution, and I is the power density of the NIR laser.

2.5. In vitro evaluation on biocompatibility of PANI:PSS

In vitro hemolysis experiments: Arterial blood of Wistar rats was collected and anticoagulated with heparin. After washing the anticoagulated blood by centrifugation, a 5% red blood cell suspension was prepared by mixing with PANI:PSS samples of gradient concentrations (0.1–2.0 mg/mL). PBS was used as a negative control, and 1% Triton X-100 was used as a positive control. The mixed solution was incubated at 37 °C for 4 h, centrifuged and photographed. The supernatant was taken and the OD value at 540 nm was measured by microplate reader (Thermo Fisher, HYX-YQ0015, USA). The hemolysis rate was calculated with reference to the following formula [41].

$$Hemolysis \cdot rate \cdot (\%) \cdot = \cdot \frac{OD_{PANI} - OD_{PBS}}{OD_{Triton} - OD_{PBS}} \cdot \times \cdot 100\% \tag{6}$$

Since PANI:PSS has a strong absorption at 540 nm, the blank of PANI:PSS group was set up to remove the influence on hemolysis.

In vitro evaluation on the cytotoxicity by MTT assay: Mouse fibroblast cells (L929) and mouse embryonic fibroblast cells (NIH/3T3) were cultured in 96 well plates (100 μL per well, 5×10^4 cells/mL; log phase). After 24 h, the PANI:PSS samples with gradient concentrations (0–2.0 mg/mL) were incubated with the cells for 24 h. Thereafter, the cells were washed with PBS for 3 times and incubated with CCK8 for another 4 h. Finally, the absorption at 450 nm was measured by a microplate reader to evaluate the cytotoxicity of PANI:PSS.

2.6. Bacterial culture and preparation

Gram-positive *Staphylococcus aureus* (*S. aureus*), *Methicillin-resistant Staphyl-ococcus aureus* (*MRSA*) and Gram-negative bacteria *Escherichia coli* (*E. coli*) were shaken overnight at 37 °C in LB medium (12 h in culture). The OD_{600} values of *S. aureus*, *MRSA* and *E. coli* suspensions were diluted to 1 for further using. LB medium preparation (per 100 mL): dd H_2O, NaCl 1.0 g, yeast extract 0.5 g, tryptone 1.0 g, high temperature sterilization.

2.7. Investigations on bacterial cell membrane integrity

SEM and TEM characterizations: The bacteria suspension (OD_{600} = 0.2, 1, 4) were incubated with PANI:PSS dissolved in PBS (0.5 mg/mL) for 30 min, followed by NIR laser irradiation (808 nm, 1.0 W/cm^2, 5 min). Then the bacteria were washed with PBS, fixed with 2.5% glutaraldehyde for 4 h, and washed 3 times with PBS, dehydrated with 30%, 50%, 70%, 90%, 100% ethanol solution for 15 min insubsequence, and dried at room temperature for 12 h (the same as above for the non-irradiated group). Gold was sprayed and scanning electronic microscope (FESEM; JEOL, JSM-6700F; Japan) was used to observe the morphological changes of the bacterial membrane.

For transmission electron microscopy (TEM; JEOL, JEM-1200EX; Japan) characterizations, the bacteria sample (~10 μL) was dropped on the front of the copper mesh to cover the entire surface of the mesh, and then allowed to stand for 5 min. The filter paper was placed close to the edge of the copper mesh and the excess sample was sucked away. According to the situation, it was washed twice with PBS. Then uranyl acetate solution (10 μL) was dropped on the front of the copper mesh. After standing for 5 min, the excess dye solution was sucked away, and the samples were placed in a drying tank for 12 h before TEM imaging.

2.8. Investigations on mammalian cell membrane translocation of water-soluble PANI:PSS

HeLa cell line was used as a mammalian cell model to investigate whether the prepared PANI:PSS can translocate across the mammalian membranes. Log-phase cells were collected, the concentration of the cell suspension was adjusted, and the cells were planted in a confocal culture dish and incubated for 24 h. And the culture medium was replaced with DMEM medium diluted PANI:PSS (20 μg/mL), incubated for 4 h. Then the medium was discarded, the dish was washed twice with PBS, and the paraformal-dehyde was added to fix the cells. Finally, HeLa cell nuclei were stained with DAPI and the penetration of the material through the membrane was observed by a laser confocal microscope.

2.9. In vitro photothermal antibacterial mediated by PANI:PSS

Plate cloning: The bacterial suspension with $OD_{600} = 1$ (1×10^9 CFU/mL) was mixed with PANI:PSS to make the final PANI:PSS concentration 0.5 mg/mL. After incubation for 1 h, the bacteria suspension was irradiated with NIR irradiation (808 nm, 1.0 W/cm^2, 5 min). The mixed solution was diluted 10^5-fold, and spread on the solid medium in a 37 °C incubator for 24 h. Finally, the number of colonies on each agar plate were calculated. Solid medium preparation (per 100 mL): dd H_2O, NaCl 1.0 g, yeast extract 0.5 g, tryptone 1.0 g, agar powder 1.5 g, high temperature sterilization.

Live/Dead staining: The bacterial suspensions were concentrated to $OD_{600} = 5$, mixed with PANI:PSS (0.5 mg/mL) and incubated for 1 h, then irradiated with NIR irradiation (808 nm, 1.0 W/cm^2, 5 min). The mixed bacteria suspension was washed 3 times with 1 × Assay Buffer to prepare a cell suspension, mixed with the staining solution in a volume ratio of 2:1, incubated at 37 °C for 1 h, and quickly analyzed by an inverted fluorescence microscope (Leica, DMI 6000B, Japan). In the dark, Calcein-AM solution (5 μL, 4 μM) and PI solution (15 μL, 4.5 μM) were added to 5 mL of 1 × Assay Buffer and mixed thoroughly. Calcein-AM stains live bacteria with yellow-green fluorescence ($\lambda_{EX} = 490$ nm, $\lambda_{EM} = 515$ nm). PI stains dead bacteria with red fluorescence ($\lambda_{EX} = 535$ nm, $\lambda_{EM} = 617$ nm).

Confocal laser scanning microscopy (CLSM) characterization: The bacterial suspensions were concentrated to $OD_{600} = 4$, and incubated with PANI:PSS (0.5 mg/mL) (37 °C, 220 rpm) for 30 min. After washing three times by centrifugation with PBS, the bacteria were resuspended with DAPI solution (1.0 mL, 10 μg/mL) at room temperature for 5 min. Finally, the samples were washed twice with PBS for confocal imaging by CLSM (Nikon, ECLIPSE Ti2-E; Japan). DAPI stains bacterial DNA with red fluorescence ($\lambda_{EX} = 345$ nm, $\lambda_{EM} = 455$ nm). PANI:PSS spontaneously emits green fluorescence ($\lambda_{EX} = 339$ nm, $\lambda_{EM} = 468$ nm).

2.10. Anti-bacterial biofilm analysis

Bacterial biofilm preparation: The bacteria suspensions (1.0 mL, $OD_{600} = 1$) were placed in 20 mm confocal glass bottom dishes and allowed to stand for 2 h at 37 °C to adhere to the bottom. After careful washing 3 times with PBS, LB medium was added to the petri dishes for further incubation at 37 °C, and the medium was changed every 24 h. Three days later, the average thickness of the bacterial biofilms reached about 15 μm. Eventually, the biofilms were washed 3 times with PBS for using [23].

Crystal violet staining method: PANI:PSS dissolved in PBS (1.0 mL, 0.5 mg/mL) was added into the bacterial biofilms for NIR irradiation (808 nm, 1.0 W/cm^2, 5 min). Thereafter, the plates were further incubated (37 °C, 24 h). After washing twice with PBS, methanol (500 μL) was immediately added to fix the bacteria (4 °C, 20 min). Then the bacterial biofilms were dyed by crystal violet (500 μL, 0.1%, RT, 30 min), washed three times with PBS. After that, ethanol (500 μL) was added to each well at room temperature with shaking for 30 min. Finally the absorption at 550 nm of the solutions were measured, and the stained images were recorded by a digital camera [42].

Evaluation on bacterial biofilm elimination by CLSM: After the PANI:PSS and bacteria mixture was further incubated for 6 h, Calcein-AM (5 μL) and PI (10 μL) were added to the bacterial biofilms and incubated for 40 min in the dark. And then, the fluorescence images of bacterial biofilm samples were recorded by CLSM.

2.11. In vitro investigations on side effects of PTA mediated by water-soluble PANI:PSS

L929 cell line was used as a normal mammalian cell model to investigate the side effects caused by the photothermal antibacterial therapy. L929 cells seeded in a 96-well plate were incubated with PANI:PSS (15.625–250 μg/mL in DMEM) for 4 h. Then the cells were washed by PBS to expel extra PANI:PSS, and irradiated by the 808 nm laser with a power density of 0.75 W/cm^2 for 5 min. Afterwards, cell death rates were measured by MTT assay.

2.12. In vivo photothermal antibacterial mediated by PANI:PSS

Establishment of *in vivo* wound model: ICR mice (with an average weight of 20.0 g) were selected for the experiment in an SPF animal room. ICR mice were shaved at 6 weeks of age. After the mice were anesthetized, round surgical incisions were made on one side of their right hind limbs by using a circular blade with a diameter of 1 cm, which conforms to the experimental animal and moral standards. Then, each wound was covered with bacterial suspensions (100 μL, 5×10^8 CFU/mL) of *MRSA* ($OD_{600} = 0.2$) or *S. aureus* ($OD_{600} = 0.5$), and was wrapped with gauze. After 24 h, all mice were randomly divided into four groups (5 mice in each group): control, NIR-only, PANI:PSS-only and PANI:PSS + NIR.

In vivo photothermal antibacterial protocol mediated by PANI:PSS: On the first day after the wound model was established, PANI:PSS dissolved in PBS (0.5 mg/mL, 100 μL) were added drop-wisely to the wound sites of ICR mice in PANI:PSS-only and PANI:PSS + NIR groups. Then the mice in NIR-only and PANI:PSS + NIR groups were irradiated with NIR laser (808 nm, 0.75 W/cm^2, 5 min). At an interval of 20 s, the thermal imager (Fluke, Ti200) was used to capture images of the wounds. Finally, the time-temperature curve of NIR laser irradiation was drawn. For the mice in NIR group, the wounds were treated with PBS (100 μL) and then exposed to laser irradiation. The mice treated simply by PBS (100 μL) on the first day served as the control group. From the next day, pictures of the mice wounds were taken daily to calculate the wound area for seven consecutive days. Then the mice were euthanized and the main organs and wound parts were collected. And the wounds were mashed to homogenize, diluted 5000-fold with PBS, and applied a volume of 100 μL to the agar plates followed by incubation at 37 °C for 24 h. Colonies were counted and imaged. And then, the collected mice wound tissues were fixed with 4% formaldehyde and embedded by optimal cutting temperature compound (OCT) to make frozen pathological sections. The wound sites were stained by H&E and Masson's trichromem [43]. Finally, histological analysis of tissue images was performed by an optical microscope (Leica, DM2000, Japan).

Immunofluorescence staining for inflammatory factor analysis: The frozen sectioned wound tissues were warmed to room temperature for 15 min, and then infiltrated with PBS for 10 min to remove the OCT. The slices were infiltrated with BSA (1%) for 1 h, and infiltrated with IL-6 at 4 °C overnight. After rinsing with PBS for 3 times, the secondary antibody was added at room temperature and the samples were put in dark for 1 h, and then rinsed with PBS. The slices were dried and mounted with DAPI mounting medium, put in dark at room temperature overnight, and then observed with an inverted fluorescence microscope (Leica, DMI 6000B, Japan).

2.13. In vivo evaluation on biocompatibility of PANI:PSS

After establishing the mice wound model, the mice body weight changes were recorded every day for one week to evaluate the safety of photothermal antibacterial treatment mediated by PANI:PSS. After that, the main organs of the mice including heart, liver, spleen, lung, and kidney were collected, fixed and embedded to prepare paraffin sections, which were stained by H&E to further evaluate the *in vivo* biocompatibility of the PANI:PSS protocol. In addition, routine blood parameters such as white blood cells (WBC), red blood cells (RBC), hemoglobins (HGB), hematocrit (HCT), mean corpuscular hemoglobin (MCH), mean corpuscular volume (MCV), mean corpuscular hemoglobin concentration (MCHC), platelets (PLT) and mean platelet volume (MPV) of the blood collected from the vein of the mice were also detected.

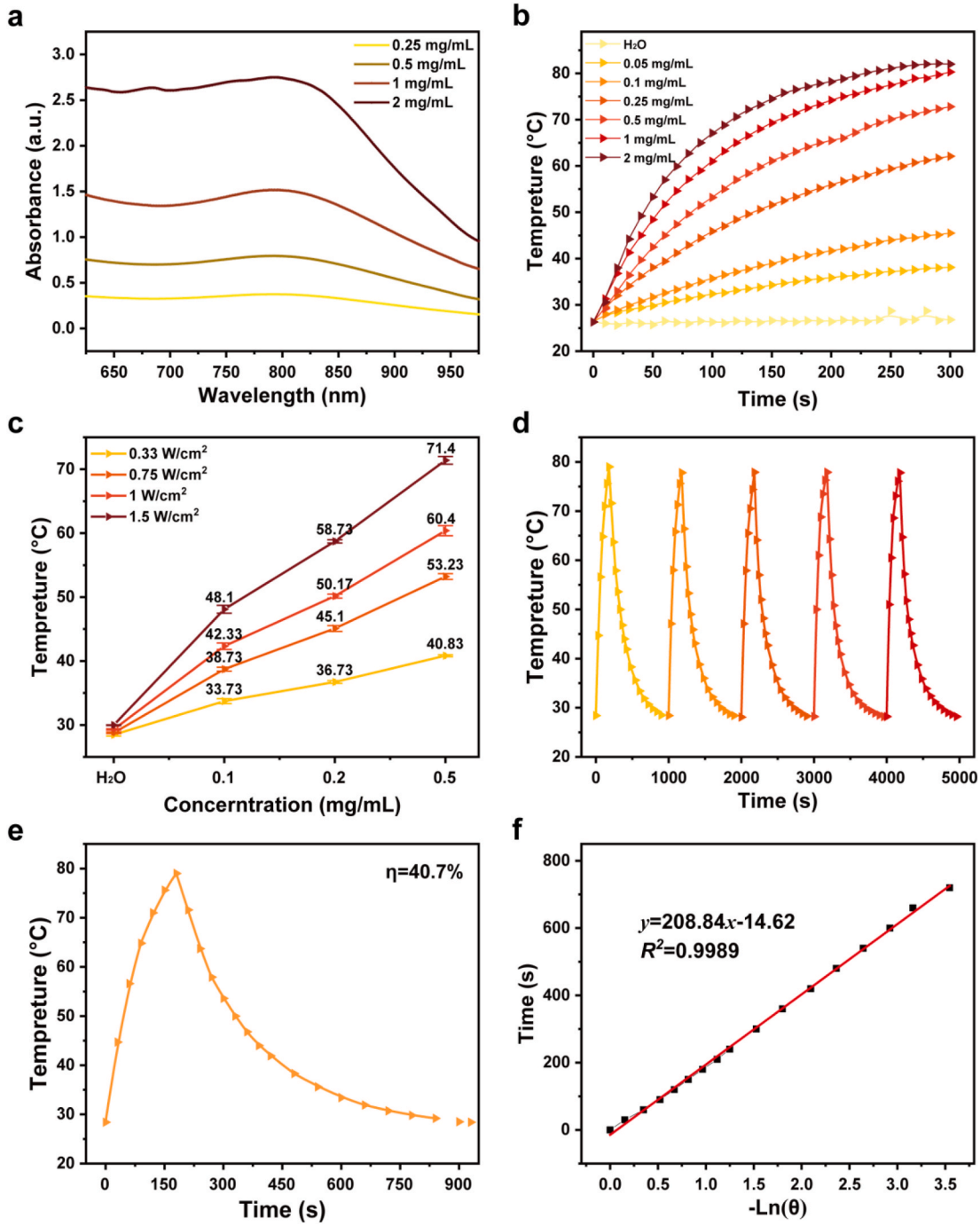

Fig. 1. (a) UV–Vis–NIR spectra and (b) heating curves under 808 nm laser irradiation (1.5 W/cm^2, 5 min) of PANI:PSS aqueous solutions with gradient concentrations. (c) The influence of concentration and laser power density (808 nm, 5 min) on the temperature of PANI:PSS aqueous solutions. (d) Photothermal cycle of PANI:PSS aqueous solution (2.0 mg/mL) under 808 nm laser irradiation (1.0 W/cm^2, 5 min). (e) and (f) Calculation of the photothermal conversion efficiency of PANI:PSS (808 nm, 1.0 W/cm^2, 5 min).

2.14. Statistical analysis

Quantified data were expressed by the mean and standard deviation (SD). Statistical analysis was performed by using independent sample T test. The differences of the data were considered to be significant where $^*p < 0.05$, $^{**}p < 0.01$, $^{***}p < 0.001$.

3. Results and discussion

3.1. Preparation of water-soluble PANI:PSS catalyzed by FePOs nanozyme

In this work, we synthesized water-soluble PANI:PSS with FePOs nanozyme as the catalyst. The synthesis process was green and environmentally friendly (no organic solvents, strong oxidants and only water as by-product). Fig. S1a shows UV–Vis–NIR spectra monitoring the polymerization of aniline catalyzed by FePOs. As time proceeded,

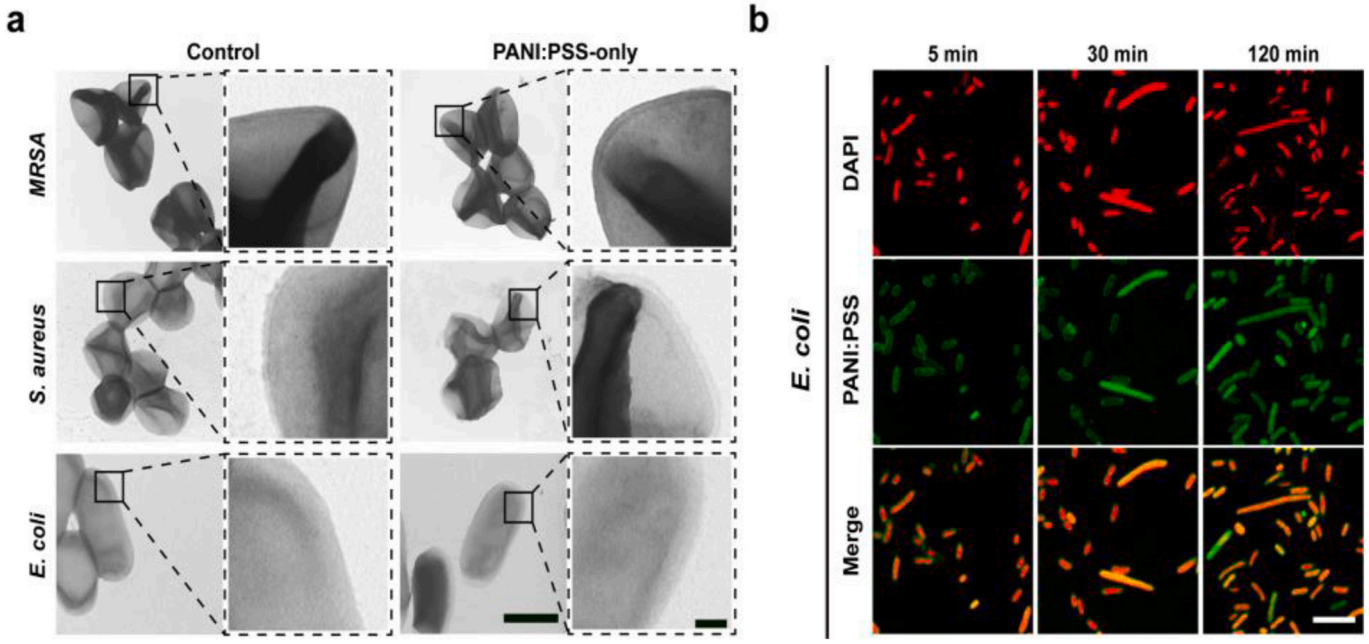

Fig. 2. (a) TEM images of *MRSA*, *S. aureus* and *E. coli* co-incubated with PANI:PSS (0.5 mg/mL) for 30 min, in which scale bars represent 1 μm (left) and 200 nm (right). (b) CLSM images of DAPI-stained *E. coli* co-incubated with PANI:PSS (0.5 mg/mL) for 5, 30 and 120 min (red: DAPI, green: PANI:PSS). Scale bars represent 5 μm.

the broad absorption band at 600–1000 nm which is compared as a signature of the formation of conductive PANI:PSS due to polaron band transitions gradually increased, indicating an increase in molecular weight of the polymer with time since the absorption of the polaron band is strongly dependent on the molecular weight and protonation level of the PANI:PSS [44].

In the FTIR spectrum (Fig. S1b) of the PANI:PSS product, the C–H out-of-plane bending at 835 cm^{-1} due to a para-substitution pattern further indicates that a head-to-tail coupling of aniline occurs during the polymerization [44,45]. The peak at 1497 cm^{-1} can be assigned to the C═C stretching vibration mode for the benzenoid rings (N–B–N) [46]. The peaks at 775 cm^{-1} and 675 cm^{-1} correspond to deformation vibration modes for the aromatic rings, while the peak at 578 cm^{-1} is characteristic for the 1,4 di-substituted benzene [47]. In addition, S═O stretching bands at 1035 and 1007 cm^{-1} confirms the presence of PSS in the complex [48]. The resulting polymer solution is dark green in color, characteristic of conductive PANI:PSS polymerized via a head-to-tail para-directed pattern (inset of Fig. S1b). The fluorescence spectra of PANI:PSS solution in Fig. S2 demonstrate that the prepared PANI:PSS emits green fluorescence centered at $\lambda_{EM} = 468$ nm with an excitation wavelength of $\lambda_{EX} = 339$ nm in agreement with the previous literatures [49], indicating the possibility of intracellular fluorescent location of the PANI:PSS.

Fig. S3 shows the characterization results of average hydrodynamic diameter of PANI:PSS, which was measured to be 42.09 nm and 14.48 nm in water and LB medium, respectively, indicating a small size suitable for membrane penetration. According to the results of Zeta potential measurement (Fig. S4), the prepared PANI:PSS was positively charged with a Zeta potential of +0.65 mV, which primes the PANI:PSS molecules for attraction by the negative charged outer leaflet and rapid membrane penetration driven by the more negatively charged inner leaflet.

3.2. Characterization of photothermal performance of PANI:PSS

In order to verify the photothermal effects of the synthesized water-soluble PANI:PSS, we evaluated the UV–Vis–NIR absorption of PANI:PSS aqueous solutions with gradient concentrations and found that the higher the PANI:PSS concentration, the stronger absorption at 808 nm (Fig. 1a). Besides, the temperature rise of PANI:PSS after NIR laser irradiation (808 nm, 1.5 W/cm^2, 5 min) was also measured. The results shown in Fig. 1b demonstrate that compared to water, the temperature increase of PANI:PSS solutions was significantly high. With an equal initial temperature of 25 °C, water was slightly heated to 26.8 °C by the laser, while the temperature of PANI:PSS solutions with gradient concentrations of 0.1–2.0 mg/mL could reach 45.5–82.0 °C, indicating the excellent photothermal properties of the prepared PANI:PSS. Fig. 1c indicates the influence of laser power density on the temperature rise of PANI:PSS. For the sample with a concentration of 0.5 mg/mL, the final temperature was alleviated from 40.8 °C to 71.4 °C if the power density increased from 0.33 to 1.5 W/cm^2. The photothermal stability of the PANI:PSS was investigated by the five laser switching cycle experiments. Fig. 1d shows that the PANI:PSS aqueous solution (2.0 mg/mL) could reach ~80 °C each time after laser irradiation for five cycles, which indicates the stability of the PANI:PSS and provides the possibility for the long-term cyclic application. With the data read from the cooling stage of the temperature rise and fall curve (Fig. 1e–f), the photothermal conversion efficiency toward 808 nm laser was calculated to be 40.7% according to Equations (1)–(5).

3.3. In vitro biocompatibility evaluation of water-soluble PANI:PSS

The biocompatibility of water-soluble PANI:PSS was evaluated through hemolysis experiment and cytotoxicity. The results in Fig. S5a show that even if the PANI:PSS concentration reached 0.5 mg/mL, the hemolysis rate was only 2.77%, similar to that of the negative control PBS group. A hemolysis rate less than 3% was considered non-hemolysis, indicating that PANI:PSS has superb biocompatibility. Then the cytotoxicity of PANI:PSS to mice normal cells L929 and 3T3 was evaluated (Fig. S5b). In the PANI:PSS concentration range from 0.1–0.5 mg/mL, the cell survival rate of all groups exceeded 80%, further verifying the excellent biocompatibility of PANI:PSS.

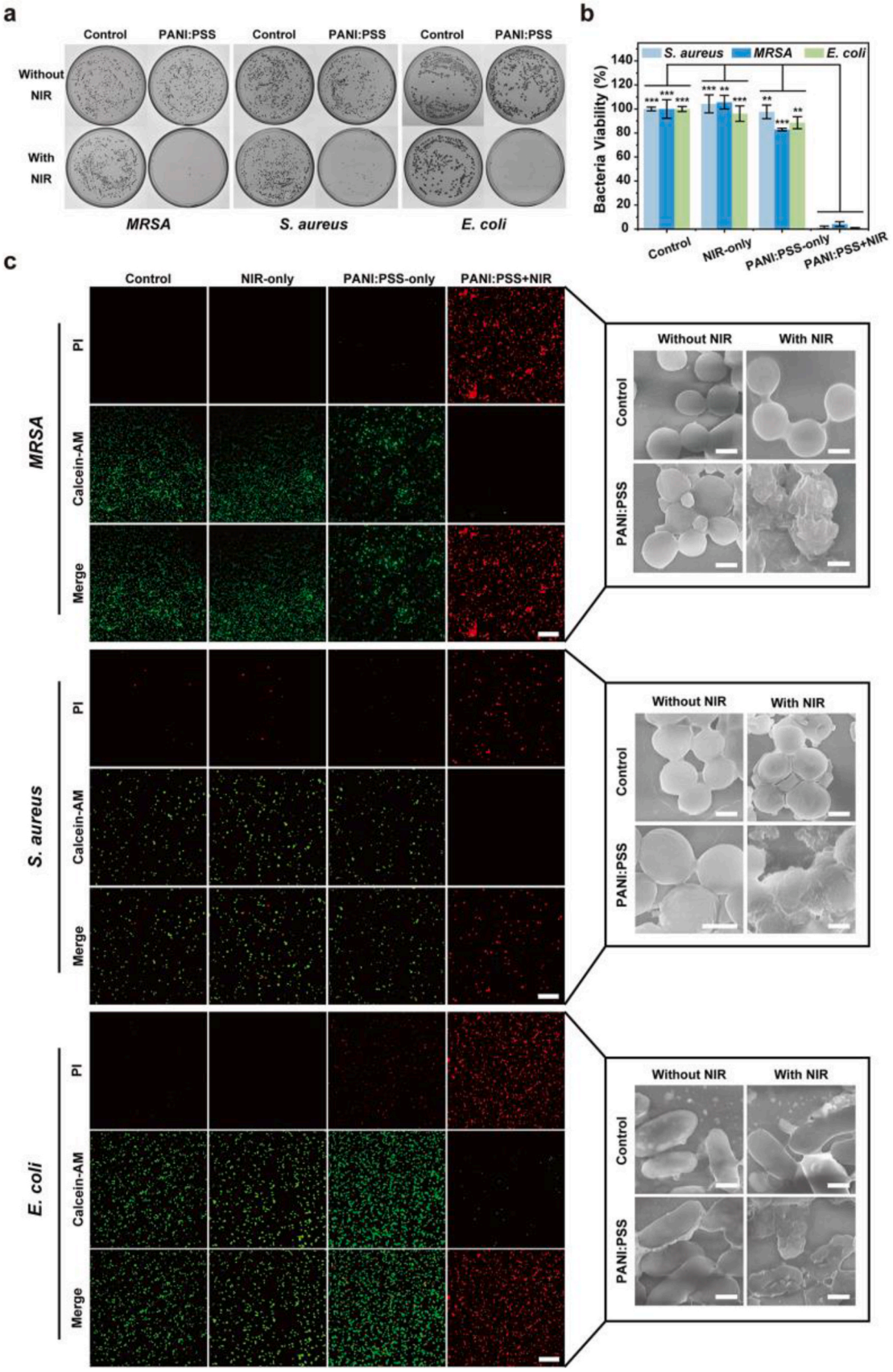

Fig. 3. (a) Photographs of bacterial colonies and (b) viability data of *MRSA*, *S. aureus* and *E. coli* after coating the plate and incubating for 18 h. Data are expressed as mean ± standard deviation (n = 3). ** represents $p < 0.01$ and *** represents $p < 0.001$. (c) Calcein-AM/PI dual staining fluorescence images captured by CLSM (red: PI, green: AM) and SEM images of *MRSA*, *S. aureus* and *E. coli*. Scale bars of CLSM images and SEM images represent 20 μm and 500 nm, respectively. NIR laser dose: 808 nm, 1.0 W/cm^2, 5 min.

3.4. Non-disruptive translocation across bacterial cell membranes of water-soluble PANI:PSS

To investigate whether PANI:PSS can translocate across bacterial cell membranes, morphological characterizations on bacterial were performed by TEM according to the method reported in literatures [19,50,51]. The morphologies of bacteria were examined after treating with PANI:PSS for 30 min. Images in Fig. 2a show that compared to pristine bacterial in control group, negligible levels of damage were observed for all the three types of bacterial after incubation with PANI:PSS at relevant working conditions. The membranes of the bacteria in PANI:PSS group remained intact and smooth without overt membrane disruption/poration observed for disruptive membrane penetration [17], indicating the non-disruptive translocation across bacterial cell membranes of the prepared water-soluble PANI:PSS owing to its amphiphilicity as we anticipated.

Based on its fluorescent properties, we performed fluorescent localization of PANI:PSS in bacteria. The bacteria were incubated with PANI:PSS for different time intervals, stained by DAPI and then washed by PBS to remove the extra PANI:PSS and DAPI before fluorescent imaging. The intracellular localization of PANI:PSS was visualized due to its green fluorescence. Results are summarized in Figs. 2b and S6, which show the CLSM images of bacteria with red color for DAPI, green for PANI:PSS, and yellow for the merged color of red and green. As shown, the process of PANI:PSS entry into bacteria cells was elegantly illustrated by the fluorescent images. It is clear to observe that PANI:PSS could label the cell membrane of *E. coli* within only 5 min. In the merged image, the rod-like outline typical of *E. coli* cells was well depicted by the green fluorescence of PANI:PSS, which suggests the localization of PANI:PSS in the cell membrane. In the next 2 h, time-dependent internalization of PANI:PSS by *E. coli* cells was confirmed by the gradually enhanced green fluorescence and yellow color in a way. Notably, we didn't observe significant PANI:PSS retention in cell membrane within 2 h, signifying that the interactions between PANI:PSS and bacteria cell membrane didn't originate from the electro-static actions. This is very important to minimize the side effects on normal mammalian cells caused by membrane disturbances involved in traditional positively charged antibacterial agents. It has been extensively reported that interactions between positive drugs and negative membranes cause membrane disturbances including membrane thinning, poration and even rupture, which inspired the development of so called "membrane targeting antibacterial agents" [17–19,51,52]. The inevitable side effects on normal mammalian cells are the main concern related to traditional cationic disinfectants, in spite of their efficiency in combating multidrug-resistance. Moreover, we neither observed leaked DNA molecules which could be labeled red by DAPI outside bacteria cells, further providing evidences that PANI:PSS could realize spontaneous non-disruptive membrane penetration.

During the past decades, some cell-penetrating peptides (CPPs) and antimicrobial peptides (AMPs) have been found to interact strongly with the membrane surface, penetrating or altering its permeability. However, the mechanism is still not unknown even after a plethora of experimental and simulation studies [53]. Nevertheless, we struggled to ascribe the mechanism of non-disruptive penetration in current work to the amphiphilic and polyelectrolyte features of the PANI:PSS after careful review of numerous literatures. On one hand, amphiphilic strategy, which was inspired by the transmembrane proteins characterized by amphiphilic nature, has been proved to be an effective way to realize membrane penetration. For example, Stellacci's group first reported the amphiphilic strategy to realize the spontaneous fusion of amphiphilic monolayer-protected gold nanoparticles (AuNPs) with lipid bilayers [21]. On the other hand, several water-soluble conducting polymers have been proved to be able to insert and align within lipid membranes due to their amphiphilic nature [54–56].

Based on the above literatures, we proposed the mechanism of non-disruptive membrane translocation performed by the PANI:PSS. First of all, we suppose that the PANI:PSS molecules are assembled into micelle-like configurations, in which the anionic, hydrophilic sulfonate groups pending from the PSS chains are exposed on the assembly surface, allowing membrane landing and counteract the repulsive hydration forces that would otherwise inhibit close approach of the outer membranes [57]. Then, the PANI:PSS molecules may change their configurations and the embedded cationic, hydrophobic PANI chains may be released due to the electrostatic attraction from the negative charges on membranes. Gradually, the orientation of PANI:PSS molecules may be reversed and form reverse micelle-like configurations to avoid electrostatic repulsion between anionic sulfonate groups and negatively charged outer membrane. Owing to the exposed hydrophobic groups, the reverse assemblies are easy to submerge into the lipid interior, and then move towards the inner membrane driven by the more negatively charged inner leaflet, and finally complete membrane penetration. Benefitting from their small size, the micelle-like PANI:PSS assemblies can pass through the gaps of the phospholipid molecules and realize membrane translocation in a non-disruptive mode.

3.5. Translocation across mammalian cell membranes by water-soluble PANI:PSS

The penetration of PANI:PSS across mammalian cell membranes was also studied since cell membrane translocation is also of great importance for mammalian cells from the view of drug delivery. We used HeLa cell line as a mammalian cell model and stained the cell nuclei by DAPI after the cells were incubated with PANI:PSS. Fig. S7 shows the confocal fluorescence images of the cells, in which the fluorescence of DAPI was red. As shown, bright green fluorescence of PANI:PSS was observed throughout the cytoplasm, and even in some nuclei of the HeLa cells, which verifies the translocation of PANI:PSS across the HeLa cell membranes and suggests great potential in drug delivery and photothermal therapy of tumors.

3.6. In vitro photothermal antibacterial activity of water-soluble PANI:PSS

In vitro antibacterial experiments, the plate count method was used to study the photothermal antibacterial activity of water-soluble PANI:PSS against *S. aureus*, *MRSA* and *E. coli*. Compared to control and PANI:PSS-only groups, the numbers of colonies in all the three PANI:PSS + NIR groups were significantly reduced, indicating that the growth of all the three types of bacteria was greatly inhibited (Fig. 3a). The bacterial survival rate of *MRSA*, *S. aureus* and *E. coli* was as low as 1.4 ± 1.1%, 4.1 ± 2.0%, 1.0 ± 0.1%, respectively, further demonstrating the excellent antibacterial activity of the PTA protocol (Fig. 3b). The results of bacteria morphological characterizations provide more evidences of the antibacterial effects.

The Calcein-AM/PI dual fluorescence death-and-live staining method was used to further confirm the antibacterial effects of the PTA protocol. Calcein-AM performs green fluorescent staining on live bacteria, while PI can only penetrate the damaged membrane to stain dead bacteria red. It could be seen from Fig. 3c that the control, NIR-only and PANI:PSS-only groups were mostly green fluorescence, while the PANI:PSS + NIR groups for all the three bacteria were basically red fluorescence, identifying the high antibacterial efficiency of the PTA protocol mediated by water-soluble PANI:PSS. From the SEM images of *MRSA* (Fig. 3c), it could be found that the morphology of bacteria in the control, NIR-only and PANI:PSS-only groups remained intact and uniform spherical. In contrast, the bacterial cell morphology of the PANI:PSS + NIR group was greatly changed and the cells were completely fragmented. Similar results were obtained for *S. aureus* and *E. coli*, which further prove that PANI:PSS + NIR treatment could cause severe hyperthermia injury to the bacterial.

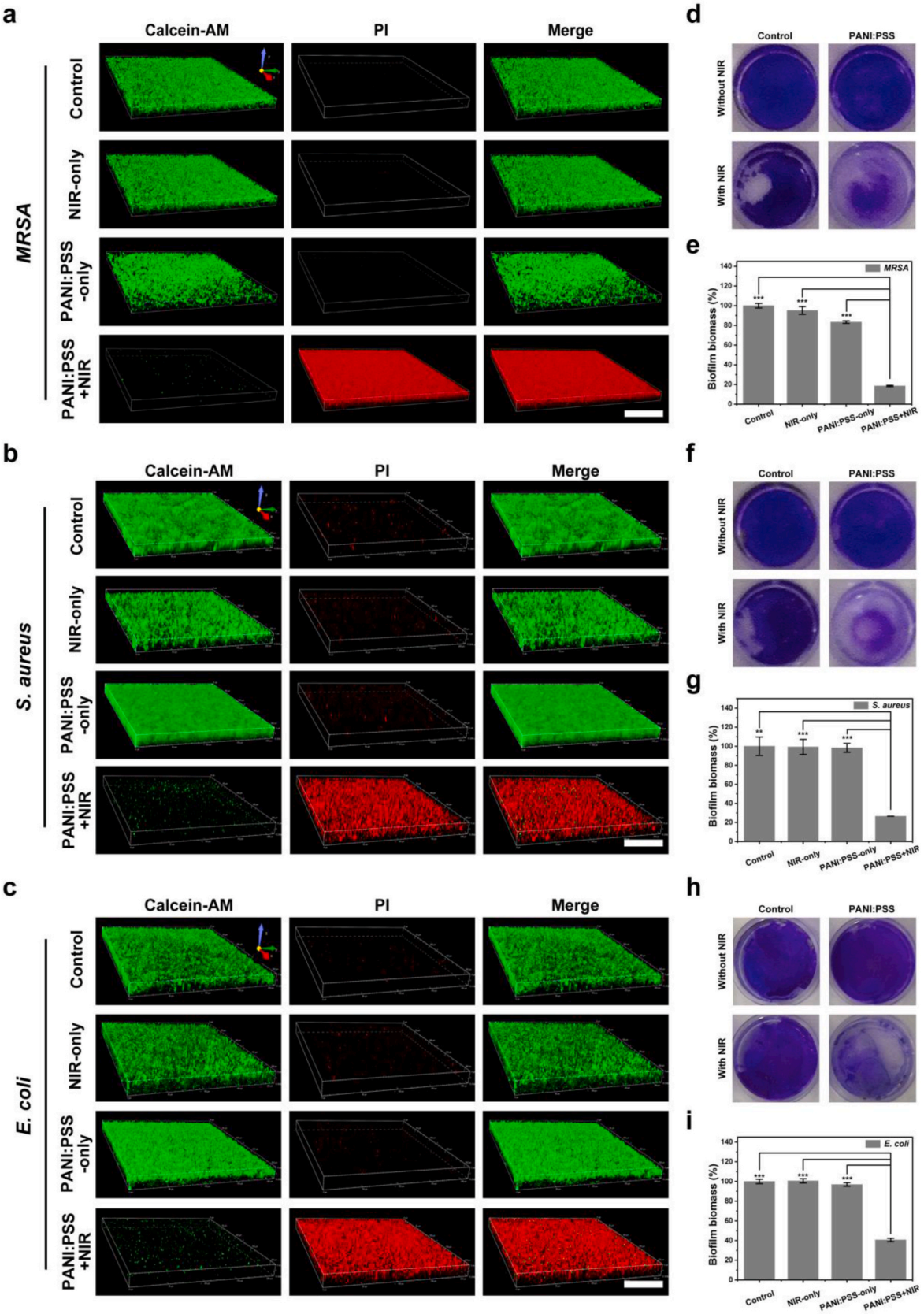

Fig. 4. Calcein-AM/PI dual staining fluorescence images of (a) *MRSA*, (b) *S. aureus* and (c) *E. coli* biofilms captured by CLSM with scale bars of 50 μm. (d–i) are images of corresponding crystal violet staining assay (d, f, h) and biomass quantification measurement (e, g, i). The average biofilm thickness was 15 μm ** represents $p < 0.01$ and *** represents $p < 0.001$.

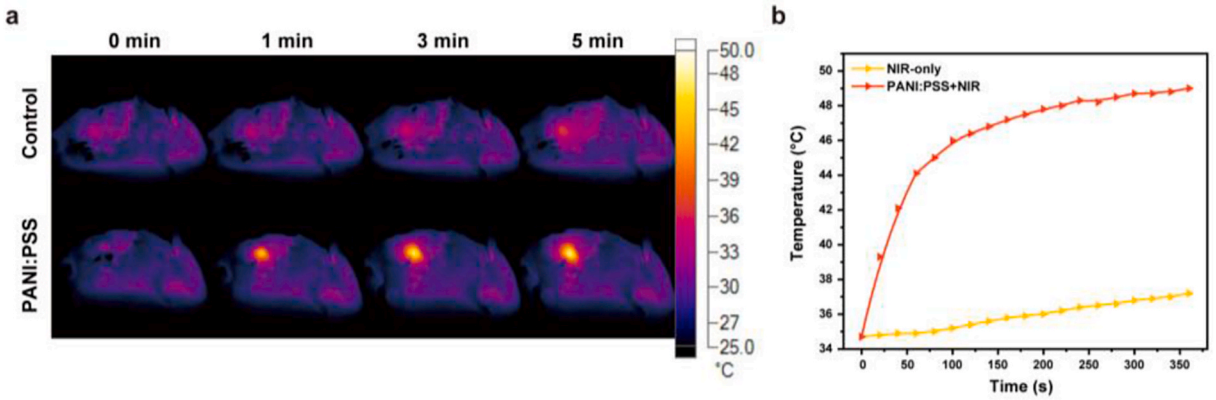

Fig. 5. (a) Infrared thermal imaging photographs of mice with wound models. (b) Shows the temperature vs. time plots recorded by the infrared thermal imaging camera. PANI:PSS dose: 0.5 mg/mL, 100 μL; 808 nm NIR laser dose: 0.75 W/cm^2, 5 min.

3.7. Anti-biofilm activity of water-soluble PANI:PSS mediated PTA

In actual antibacterial applications, most infectious diseases caused by free bacteria can be controlled quickly unless the bacterial biofilm is formed, in which the membrane structure (polymerized membrane of polysaccharide matrix, fibrin, lipid protein, etc.) is not easily penetrated by drugs [58]. Furthermore, bacterial biofilms have natural resistance to antibiotics and body immunity, making them difficult to be completely eliminated [59]. In this work, we further evaluated the anti-biofilm activity of PANI:PSS-mediated PTA.

The results of Calcein-AM/PI dual fluorescence staining shown in Fig. 4a, d and g verify that the PANI:PSS-PTA protocol could effectively eliminate the bacterial biofilm. The biofilms of the control, NIR-only and PANI:PSS-only groups all emitted bright green fluorescence which is indicative of live bacteria. On the contrary, the intense red fluorescence emitting from the PANI:PSS + NIR group biofilm definitely indicate the elimination of the bacteria as the result of the hyperthermia treatment. The amount of biofilm quantified by measuring OD_{550} (Fig. 4b–c, e-f, h-i) were in good agreement with that of Calcein-AM/PI dual fluorescence staining.

3.8. Side effects of in vitro PTA mediated by water-soluble PANI:PSS

Before carrying out *in vivo* PTA, *in vitro* side effects caused by the 808 nm laser irradiation in presence of PANI:PSS were investigated on normal mammalian cells by using L929 cell line as a cell model. As shown in Fig. S6, cell viability was higher than 70% even the PANI:PSS concentration was as high as 250 μg/mL. In addition, it is very interesting to find out that the viability of L929 cells treated by the prepared PANI:PSS was enhanced after being exposed to the 808 nm laser (0.75 W/cm^2, 5 min), which might be due to the positive effects of low-temperature phothermal treatment. It has been reported that moderate heating with temperature of 37–41 °C promotes proliferation of normal cells [14]. Moreover, the 808 nm laser was locally shed within the wound domain in practical *in vivo* PTA. Therefore, it is reasonable to conceive that the *in vitro* PTA caused minimal side effects on L929 cells.

3.9. In vivo antibacterial activity and biocompatibility evaluation of water-soluble PANI:PSS

In order to further evaluate the practical applications of water-

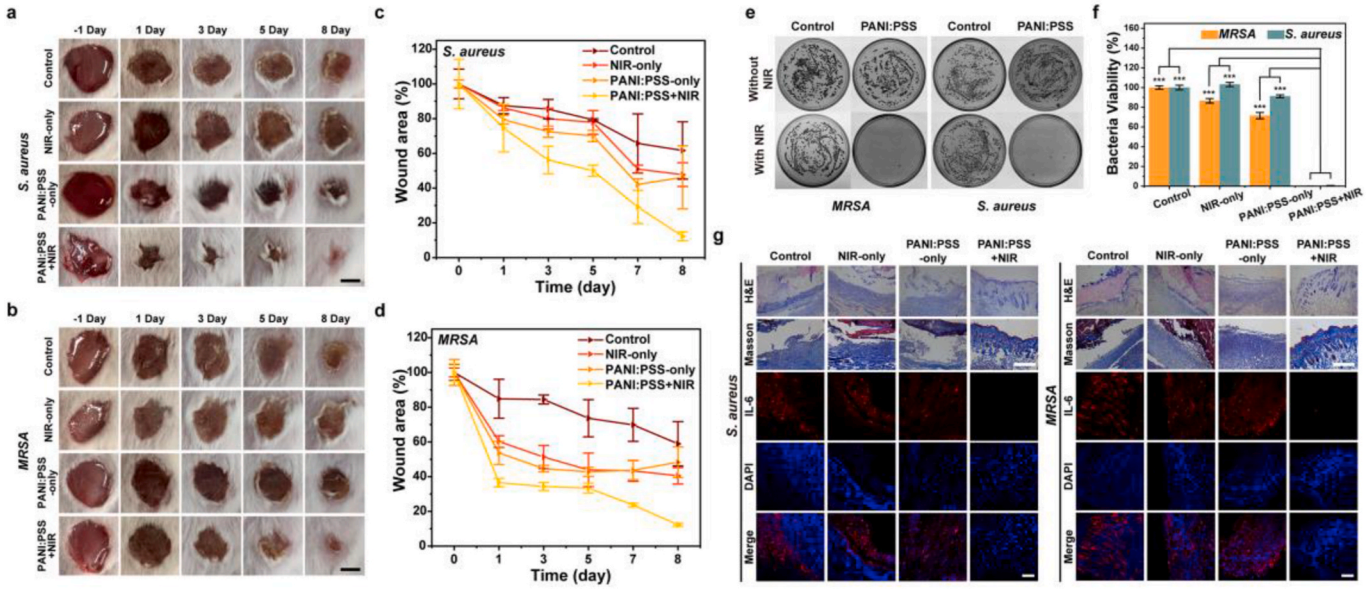

Fig. 6. (a) and (b) are photographs of *S. aureus* and *MRSA* infected wounds of control, NIR-only, PANI:PSS-only and PANI:PSS+NIR groups. Scale bars represent 5 mm. (c) and (d) show area changes of *S. aureus* and *MRSA*-infected wounds over time. (e) Photographs of agar plates and (f) survival rates of *MRSA* and *S. aureus* in the infected wound tissues. *** represents $p < 0.001$. (g) H&E-staining, Masson-staining and immune cell marker staining (IL-6) images of wound tissues after different treatments. Scale bars represent 400 μm in H&E and Masson images, while 100 μm in fluorescence images.

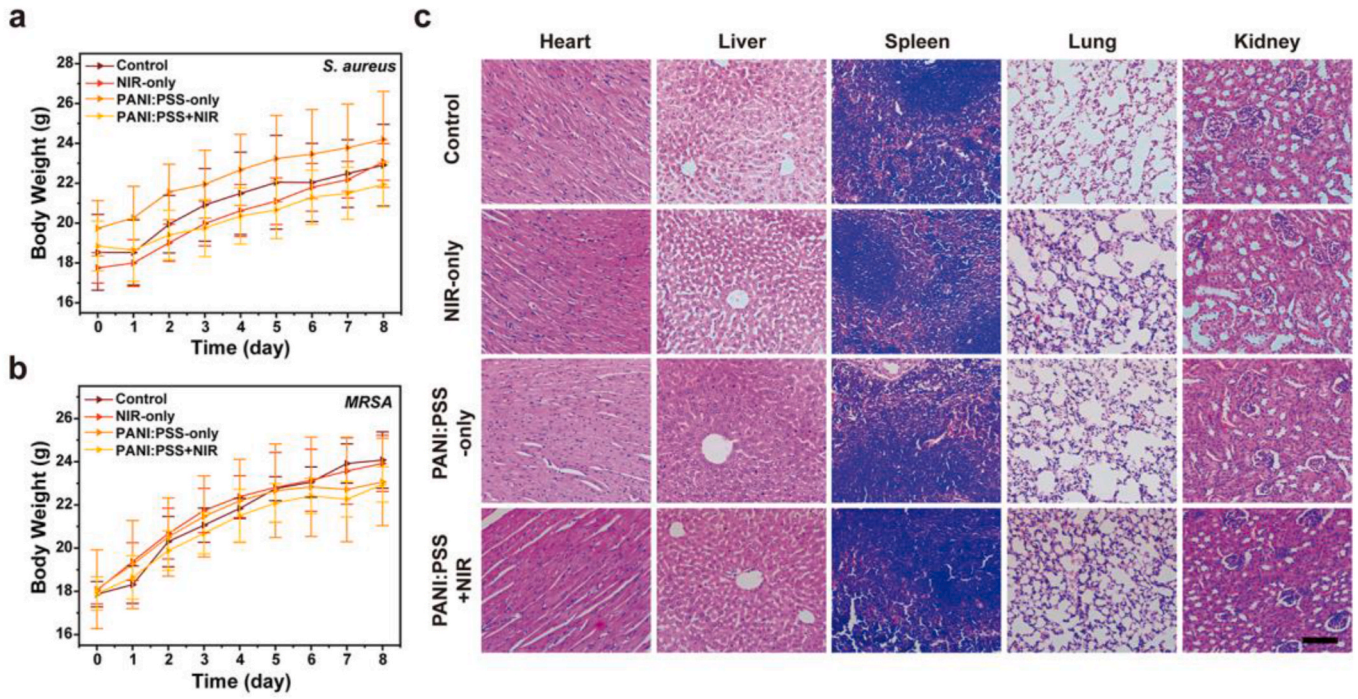

Fig. 7. Body weight change of mice infected by (a) *S. aureus* and (b) *MRSA* during the *in vivo* antibacterial therapy. (c) H&E staining photos of mice organs subjected to the *in vivo* antibacterial therapy. Scale bar: 100 μm.

soluble PANI:PSS in the treatment of bacterial wound infection, *S. aureus* and *MRSA* were used to established wound models in ICR mice. The mice were randomly divided into 4 groups, each with 5 mice, namely "Control", "NIR-only", "PANI:PSS-only" and "PANI:PSS + NIR". Correspondingly, the wounds were treated by PBS, NIR irradiation, PANI:PSS and PANI:PSS + NIR irradiation after being infected with *S. aureus* and *MRSA* for 24 h. The *in vivo* photothermal effects of PANI:PSS under 808 nm laser irradiation were recorded by an infrared thermal imaging camera. The results shown in Fig. 5a–b demonstrate that the average temperature of the wounds in PANI:PSS + NIR group reached about 49 °C, which is high enough to kill most bacterial. However, in the absence of PANI:PSS the wounds could only be heat to 37.2 °C, showing no threat to bacteria at all.

As a result, rapid healing was observed for the PANI:PSS + NIR group (Fig. 6a–b) in that the wound area reduced by ~90% within 8 days after S. *aureus* or *MRSA* infection. With other conditions equal, the wound area reduction within 8 days was no larger than 40% for the other groups (Fig. 6c–d). In order to further quantify the PTA effect of water-soluble PANI:PSS, the numbers of bacteria that survived in wound tissues were determined by colony formation assay. The skin tissues of the mice wounds were collected on the 9th day after the treatment, and the skin homogenate was resuspended, followed by bacterial dilution coating. The sharp contrast between the images of PANI:PSS + NIR and other groups (Fig. 6e) clearly identifies the excellent *in vivo* antibacterial effects of the PTA protocol against both *S. aureus* and *MRSA*. Accordingly, the bacteria viability of PANI:PSS + NIR was extremely low, which was 0.48% and 0.07% for *S. aureus* and *MRSA*, respectively (Fig. 6f).

We further assessed wound healing by histological analysis, in which the infected tissues of the mice were collected and stained with hematoxylin and eosin (H&E). The formation of collagen fibers in the wound area was studied by the Masson trichrome staining method. The results are shown in Fig. 6g. In the H&E staining images of control, NIR-only and PANI:PSS-only groups, a large number of inflammatory cells were captured, and the epithelial tissues were loose and irregular. On the contrary, in the images of PANI:PSS + NIR group, intact epidermis was observed and very few inflammatory cells could be found. The lamellar epithelial tissue was neat, the dermal tissue was orderly and a large number of blood vessels in the dermis could be seen. Correspondingly, the collagen fibers which can be stained blue by Masson were continuous and more obvious in the wound of PANI:PSS + NIR group, indicating a much better recovery than the other groups.

Immunofluorescence staining was also performed to detect the expression of the inflammatory factor, IL-6, in the wounds. The results demonstrated in the fluorescence images of Fig. 6c indicate that the pro-inflammatory-related genes in the bacterially infected wound tissues were remarkably down-regulated by the PANI:PSS + NIR treatment, further identifying the bacterial inhibition effects of the PTA protocol.

Finally, we evaluated the biocompatibility of water-soluble PANI:PSS *in vivo*. As shown in Fig. 7a and b, the weight of the mice did not decrease or fluctuate much, and maintained at a relatively stable level during the *in vivo* experiment PANI:PSS treatment. The histological images of the tissues stained by H&E (Fig. 7c) show that after PANI:PSS photothermal treatment, there was no physiological toxicity to the main organs of mice, such as the heart, liver, spleen, lung and kidney. In addition, the *in vivo* biocompatibility of PANI:PSS was further evaluated by routine blood biochemical examinations using ICR female mice as animal model. PBS and PANI:PSS solution were continuously injected into mice through tail vein once a day for 2 days. On the first and eighth day after treatment, the blood of the mice was taken for hematological marking to analyze the acute and chronic toxicity of PANI:PSS. The results in Fig. S8 demonstrate that all the blood indices of the samples, including white blood cells (WBC), red blood cells (RBC), hemoglobins (HGB), hematocrit (HCT), mean corpuscular volume (MCV), mean corpuscular hemoglobin (MCH), mean corpuscular hemoglobin concentration (MCHC), platelets (PLT) and mean platelet volume (MPV) fell into the normal range. It means that the injection of PANI:PSS did not damage blood cells or cause significant inflammation in the body. The above all further prove that the water-soluble PANI:PSS has prominent safety and feasibility for the *in vivo* photothermal antibacterial therapy.

4. Conclusions

In summary, we realized translocation across bacteria cell membranes of water-soluble PANI:PSS without overt membrane disruption/poration. Rapid entry of the PANI:PSS into bacteria cells was easily verified owing to its fluorescent properties. The amphiphilic nature was ascribed as the reason why the polymer can spontaneously penetrate bacteria cellular membranes in a non-disruptive way. An efficient antibacterial protocol with minimal side effects was developed via using the water-soluble PANI:PSS as a photothermal agent. The bacteria killing efficiency against *S. aureus*, *MRSA* and *E. coli* was significantly high since hyperthermia was generated from inside the bacteria cells by the internalized PANI:PSS, which damaged the most important biomolecules directly and caused bacteria cell death. We believe that the prepared water-soluble PANI:PSS in this study has prospective applications as a novel medical disinfectant and drug delivery vehicle.

CRediT authorship contribution statement

Huanfeng Tang: Conceptualization, Data curation, Formal analysis, Writing – original draft, Writing – review & editing. **Yifan Liu:** Data curation, Formal analysis, Investigation, Methodology, Software. **Bing Li:** Methodology, Software. **Bo Shang:** Investigation. **Jiacheng Yang:** Investigation. **Congrou Zhang:** Methodology, Software. **Lijun Yang:** Formal analysis. **Kezheng Chen:** Resources, Project administration. **Wei Wang:** Funding acquisition, Investigation, Methodology, Resources, Writing – review & editing. **Jianfeng Liu:** Funding acquisition, Investigation, Methodology, Resources, Writing – review & editing.

Declaration of competing interest

The authors declare that they have no known competing financial interests or personal relationships that could have appeared to influence the work reported in this paper.

Acknowledgements

This research was financially supported by the Natural Science Foundation of Shandong Province (CN) (grant no. ZR2018MEM016), the National Natural Science Foundation of China (81971731), the CAMS Innovation Fund for Medical Sciences (CIFMS, 2016-I2M-3–022), the Non-profit Central Research Institute Fund of Chinese Academy of Medical Sciences (2018PT35031), and the National Science Fund for Distinguished Young Scholars of Tianjin (18JCJQJC47300).

Appendix A. Supplementary data

Supplementary data to this article can be found online at https://doi.org/10.1016/j.bioactmat.2021.05.019.

References

[1] M. Baym, L.K. Stone, R. Kishony, Science 351 (2016) aad3292, https://doi.org/10.1126/science.aad3292.
[2] C.M. Courtney, S.M. Goodman, J.A. Mcdaniel, N.E. Madinger, A. Chatterjee, P. Nagpal, Nat. Mater. 15 (2016) 529, https://doi.org/10.1038/nmat4542.
[3] Y. feng, L. Liu, J. Zhang, H. Aslan, M. Dong, J. Mater. Chem. B 5 (2017) 8631, https://doi.org/10.1039/C7TB01860F.
[4] J.W. Costerton, P.S. Stewart, E.P. Greenberg, Science 284 (1999) 1318, https://doi.org/10.1126/science.284.5418.1318.
[5] J. Azeredo, N.F. Azevedo, R. Briandet, N. Cerca, T. Coenye, A.R. Costa, M. Desvaux, G. Di bonaventura, M. Hébraud, Z. Jaglic, M. Kačániová, S. Knøchel, A. Lourenço, F. Mergulhão, R.L. Meyer, G. Nychas, M. Simões, O. Tresse, C. Sternberg, Crit. Rev. Microbiol. 43 (2017) 313, https://doi.org/10.1080/1040841X.2016.1208146.
[6] Y. Zhao, X. Dai, X. Wei, Y. Yu, X. Chen, X. Zhang, C. Li, ACS Appl. Mater. Interfaces 10 (2018) 14426, https://doi.org/10.1021/acsami.8b01327.
[7] L. Shen, Y. Jiang, Q. Tang, J. Ji, B. Wang, Y. Huang, Z. Qian, J. Biomed. Nanotechnol. 13 (2017) 1069, https://doi.org/10.1166/jbn.2017.2431.
[8] K. Zheng, M.I. Setyawati, D.T. Leong, J. Xie, Coord. Chem. Rev. 357 (2018) 1. https://doi.org/10.1016/j.ccr.2017.11.019.
[9] G. Su, F. Tang, D. Chen, B. Yu, Z. Huang, Y. Luo, X. Mao, P. Zheng, J. Yu, J. Luo, J. He, Int. J. Pept. Res. Therapeut. 25 (2018) 827, https://doi.org/10.1007/s10989-018-9732-7.
[10] B. He, S. Ma, G. Peng, D. He, Nanomed. Nanotechnol. Biol. Med. 14 (2018) 365, https://doi.org/10.1016/j.nano.2017.11.002.
[11] I. Mulder, J. Siemens, V. Sentek, W. Amelung, K. Smalla, S. Jechalke, Rev. Environ. Sci. Biotechnol. 17 (2018) 159, https://doi.org/10.1007/s11157-017-9457-7.
[12] S.M. Modak, M.S. Shintre, T. Gaonkar, L. Caraos, U.S. Patent 9 (421) (2016) 263, doi.org/US7871649 B2.
[13] D.L. Zubris, K.P. Minbiole, W.M. Wuest, Curr. Top. Med. Chem. 17 (2017) 305, https://doi.org/10.2174/1568026616666160829155805.
[14] D. Jaque, L. Martínez maestro, B. Del rosal, P. Haro-gonzalez, A. Benayas, J. L. Plaza, E. Martín rodríguez, SOLé J. García, Nanoscale 6 (2014) 9494, https://doi.org/10.1039/c4nr00708e.
[15] Y.W. Lee, D.C. Luther, R. Goswami, T. Jeon, V. Clark, J. Elia, S. Gopalakrishnan, V. M. Rotello, J. Am. Chem. Soc. 142 (2020) 4349, https://doi.org/10.1021/jacs.9b12759.
[16] S. Zhao, J.W. Adamiak, V. Bonifay, J. Mehla, H.I. Zgurskaya, D.S. Tan, Nat. Chem. Biol. 16 (2020) 1293, https://doi.org/10.1038/s41589-020-00674-6.
[17] P.R. Leroueil, S.A. Berry, K. Duthie, G. Han, V.M. Rotello, D.Q. Mcnerny, J. R. Baker JR., B.G. Orr, M.M. Holl, Nano Lett. 8 (2008) 420, https://doi.org/10.1021/nl0722929.
[18] D.P. Linklater, V.A. Baulin, X. Le guével, J.B. Fleury, E. Hanssen, T.H.P. Nguyen, S. Juodkazis, G. Bryant, R.J. Crawford, P. Stoodley, E.P. Ivanova, Adv. Mater. 32 (2020), e2005679, https://doi.org/10.1002/adma.202005679.
[19] L. Zheng, J. Li, M. Yu, W. Jia, S. Duan, D. Cao, X. Ding, B. Yu, X. Zhang, F.J. Xu, J. Am. Chem. Soc. 142 (2020) 20257, https://doi.org/10.1021/jacs.0c10771.
[20] R.C. Van lehn, P.U. Atukorale, R.P. Carney, Y.S. Yang, F. Stellacci, D.J. Irvine, A. Alexander-katz, Nano Lett. 13 (2013) 4060, https://doi.org/10.1021/nl401365n.
[21] A. Verma, O. Uzun, Y. Hu, Y. Hu, H.S. Han, N. Watson, S. Chen, D.J. Irvine, F. Stellacci, Nat. Mater. 7 (2008) 588, https://doi.org/10.1038/nmat3593.
[22] Y. Jia, B. Ma, X. Wei, Z. Qian, Chin. Chem. Lett. 28 (2017) 691, https://doi.org/10.1016/j.cclet.2017.01.021.
[23] S. Wu, A. Li, X. Zhao, C. Zhang, B. Yu, N. Zhao, F.J. Xu, ACS Appl. Mater. Interfaces 11 (2019) 17177, https://doi.org/10.1021/acsami.9b01149.
[24] J.W. Xu, K. Yao, Z.K. Xu, Nanoscale 11 (2019) 8680, https://doi.org/10.1039/c9nr01833f.
[25] J. Liao, K. Shi, Y. Jia, Y. Wu, Z. Qian, Bioactive Mater. 6 (2021) 2221, https://doi.org/10.1016/j.bioactmat.2021.01.006.
[26] L. Sasso, A. Heiskanen, F. Diazzi, M. Dimaki, J. Castillo-león, M. Vergani, E. Landini, R. Raiteri, G. Ferrari, M. Carminati, M. Sampietro, W.E. Svendsen, J. Emnéus, Analyst 138 (2013) 3651, https://doi.org/10.1039/c3an00085k.
[27] J. Liao, K. Shi, Q. Ding, Y. Qu, F. Luo, Z. Qian, J. Biomed. Nanotechnol. 10 (2014) 3085, https://doi.org/10.1166/jbn.2014.1934.
[28] Z.J. Du, G.Q. Bi, X.T. Cui, Adv. Funct. Mater. 28 (2018), 1703988, https://doi.org/10.1002/adfm.201703988.
[29] B. Zhu, Y. Li, F. Huang, Z. Chen, J. Xie, C. Ding, J. Li, Biomater. Sci. 7 (2019) 4730, https://doi.org/10.1039/c9bm01203f.
[30] S.B. Abel, E.I. Yslas, C.R. Rivarola, C.A. Barbero, Nanotechnology 29 (2018), 125604, https://doi.org/10.1088/1361-6528/aaa99a.
[31] M. Ghaffari-moghaddam, H. Eslahi, Arab. J. Chem. 7 (2014) 846, https://doi.org/10.1016/j.arabjc.2013.11.011.
[32] M.B. Tabatabai, M. Mirjalili, F. Yazdiyan, S. Hekmatimoghaddam, Proc. Natl. Acad. Sci. India B Biol. Sci. 89 (2018) 1109, https://doi.org/10.1007/s40011-018-1025-6.
[33] C. Korupalli, P. Kalluru, K. Nuthalapati, N. Kuthala, R. Vankayala, Bioengineering 7 (2020) 94, https://doi.org/10.3390/bioengineering7030094.
[34] H. Wei, E. Wang, Chem. Soc. Rev. 42 (2013) 6060, https://doi.org/10.1039/c3cs35486e.
[35] W. Wang, X. Jiang, K. Chen, Chem. Commun. 48 (2012) 7289, https://doi.org/10.1039/c2cc32429f.
[36] L. Yang, C. Zhang, F. Huang, J. Liu, Y. Zhang, C. Yang, C. Ren, L. Chu, B. Liu, J. Liu, J. Contr. Release 324 (2020) 354, https://doi.org/10.1016/j.jconrel.2020.05.034.
[37] H. Strahl, L.W. Hamoen, Proc. Natl. Acad. Sci. U. S. A 107 (2010) 12281, https://doi.org/10.1073/pnas.1005485107.
[38] L. Li, K. Liang, Z. Hua, M. Zou, K. Chen, W. Wang, Polym. Chem. 6 (2015) 2290, https://doi.org/10.1039/c4py01716a.
[39] Q. Cai, J. Xu, D. Yang, Y. Dai, G. Yang, C. Zhong, S. Gai, F. He, P. Yang, J. Mater. Chem. B 6 (2018) 8148, https://doi.org/10.1039/C8TB02407C.
[40] Z. Hua, B. Li, L. Li, X. Yin, K. Chen, W. Wang, J. Phys. Chem. C 121 (2016) 60, https://doi.org/10.1021/acs.jpcc.6b08975.
[41] X. Zhang, C. Ren, F. Hu, Y. Gao, Z. Wang, H. Li, J. Liu, B. Liu, C. Yang, Anal. Chem. 92 (2020) 5185, https://doi.org/10.1021/acs.analchem.9b05704.
[42] X. Jia, I. Ahmad, R. Yang, C. Wang, J. Mater. Chem. B 5 (2017) 2459, https://doi.org/10.1039/c6tb03084j.
[43] C. Cao, W. Ge, J. Yin, D. Yang, W. Wang, X. Song, Y. Hu, J. Yin, X. Dong, Small 16 (2020), e2000436, https://doi.org/10.1002/smll.202000436.
[44] Q. Wang, Z. Yang, X. Zhang, X. Xiao, C.K. Chang, B. Xu, Angew. Chem. Int. Ed. 46 (2007) 4285, https://doi.org/10.1002/ange.200700404.
[45] X.Q. Zhang, S.W. Gong, Y. Zhang, T. Yang, C.Y. Wang, N. Gu, J. Mater. Chem. 20 (2010) 5110, https://doi.org/10.1039/c0jm00174k.
[46] J. Tang, X. Jing, B. Wang, F. Wang, Synth. Met. 24 (1988) 231, https://doi.org/10.1016/0379-6779(88)90261-5.
[47] Z. Chen, C. Della pina, E. Falletta, M. Rossi, J. Catal. 267 (2009) 93, https://doi.org/10.1016/j.jcat.2009.07.007.

[48] Q. Wang, Z. Yang, X. Zhang, X. Xiao, B. Xu, Angew. Chem. Int. Ed. 46 (2010) 4285, https://doi.org/10.1002/anie.200700404.
[49] K.G.B. Alves, E.F. De melo, C.A.S. Andrade, C.P. De melo, J. Nanoparticle Res. 15 (2013) 1339, https://doi.org/10.1007/s11051-012-1339-x.
[50] T.N. Siriwardena, M. Stach, R. He, B.H. Gan, S. Javor, M. Heitz, L. Ma, X. Cai, P. Chen, D. Wei, H. Li, J. Ma, T. Köhler, C. Van delden, T. Darbre, J.L. Reymond, J. Am. Chem. Soc. 140 (2017) 423, https://doi.org/10.1021/jacs.7b11037.
[51] T. Galbadage, D. Liu, L.B. Alemany, R. Pal, J.M. Tour, R.S. Gunasekera, J.D. Cirillo, ACS Nano 13 (2019) 14377, https://doi.org/10.1021/acsnano.9b07836.
[52] S. Gao, X. Yan, G. Xie, M. Zhu, X. Ju, P.J. Stang, Y. Tian, Z. Niu, Proc. Natl. Acad. Sci. U. S. A 116 (2019) 23437, https://doi.org/10.1073/pnas.1911869116.
[53] S. De, P. Seal, S. Parekh, R. Tupally, C. Smith, Advanced Theory Simulation 3 (2020), 1900152, https://doi.org/10.1002/adts.201900152.
[54] L.E. Garner, J. Park, S.M. Dyar, A. Chworos, J.J. Sumner, G.C. Bazan, J. Am. Chem. Soc. 132 (2010) 10042, https://doi.org/10.1021/ja1016156.
[55] H. Hou, X. Chen, A.W. Thomas, C. Catania, N.D. Kirchhofer, L.E. Garner, A. Han, G. C. Bazan, Adv. Mater. 25 (2013) 1593, https://doi.org/10.1002/adma.201204271.
[56] Y. Zhang, S. Inal, C.-Y. Hsia, M. Ferro, M. Ferro, S. Daniel, R. Owens, Adv. Funct. Mater. 26 (2016) 7304, https://doi.org/10.1002/adfm.201602123.
[57] M.A. Tahir, Z.P. Guven, L.R. Arriaga, B. Tinao, Y.S. Yang, A. Bekdemir, J.T. Martin, A.N. Bhanji, D. Irvine, F. Stellacci, A. Alexander-katz, Proc. Natl. Acad. Sci. U. S. A 117 (2020) 18470, https://doi.org/10.1073/pnas.1902597117.
[58] M. Jamal, W. Ahmad, S. Andleeb, F. Jalil, M. Imran, M.A. Nawaz, T. Hussain, M. Ali, M. Rafiq, M.A. Kamil, J. Chin. Med. Assoc. 81 (2018) 7, https://doi.org/10.1016/j.jcma.2017.07.012.
[59] M. Liu, T. Liu, X. Zhang, Z. Jian, H. Xia, J. Yang, X. Hu, M. Xing, G. Lou, J. Wu, Int. J. Nanomed. 14 (2019) 3345, https://doi.org/10.2147/IJN.S199618.